ACS Macro Letters

Letter

pubs.acs.org/macroletters

Segmental Dynamics of Polymer Melts with Spherical Nanoparticles

Shushan Gong,[†,‡] Quan Chen,[†,‡] Joseph F. Moll,[§] Sanat K. Kumar,[§] and Ralph H. Colby*[,‡]

[‡]Department of Materials Science and Engineering, Pennsylvania State University, University Park, Pennsylvania 16802 United States

[§]Department of Chemical Engineering, Columbia University, 500 W 120th Street New York, New York 10027 United States

Supporting Information

ABSTRACT: The impact of spherical nanoparticles (NPs) on the segmental dynamics of polymer melts is investigated. The addition of NPs broadens the segmental dynamics with effects of both particle size and loading. Interfacial bound layer thickness is calculated by the difference in magnitude of the segmental dynamics of pure polymer and nanocomposites. These theoretical models suggest that the bound layer thickness in the case of strongly adsorbing polymer matrices may increase with particle size.

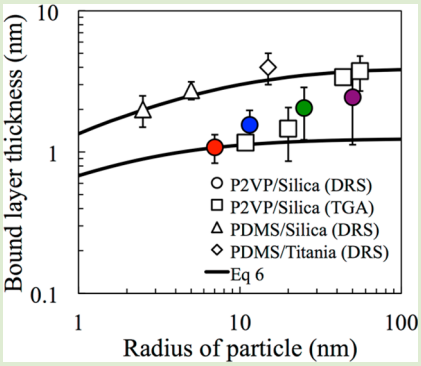

Some physical properties (e.g., mechanical, electrical, thermal, and barrier properties) of polymers are dramatically altered by the addition of nanofillers.[1] While the exact mechanism of these changes is still controversial, there is a general agreement that the polymer−filler interaction, which is concentrated in a region near the polymer−filler interface, is crucial.[2] Various experimental techniques (e.g., differential scanning calorimetry, dielectric relaxation spectroscopy, and thermally stimulated depolarization current)[3] suggest the existence of an interfacial region by observing decreases in the polymer chains' dynamic mobility with the introduction of nanoparticles. The presence of the interfacial region is often attributed to enthalpic attraction between the hydroxyl groups on the filler surface and specific groups on the polymer chain.[3] The layer of polymers affected by the nanoparticle is within a few nanometers from the filler surface. Therefore, experimentally resolving this dynamic change is challenging.

Addition of nanofillers has been reported to have a negligible influence on the local segmental relaxation function and relaxation times of polymer matrices.[4] Recent studies have shown that the curvature of nanoparticles affects the interactions between polymers and nanofillers and, thus, affects the bound polymer layer.[5−7] In 1974, Meissner used a random-process model to estimate the processes involved in the polymer−filler interaction, discussing the changes of bound layer thickness with filler concentration, filler surface area, and reactivity of the filler surface.[8] Garvey et al. stated that the volume per surface area of the bound layer decreases with increasing curvature, by assuming the bound layer mass per surface area is independent of curvature.[9] Baker et al. further illustrated that larger curvature allows more polymer segments to access and be immobilized by the surface.[10] Harton et al. used mean-field theory to predict that the bound layer thickness could decrease by a factor of 2 when the planar surfaces are reduced to small nanoparticles.[7] Clearly, bound polymer layer thickness is influenced by particle size. However, unless the thickness is comparable to the particle size, the curvature effect should not too significantly influence the bound layer thickness. Klonos et al. found that the bound layer thickness for titania/poly(dimethylsiloxane) (PDMS) nanocomposites is twice as large as that for PDMS/silica nanocomposites, which they attributed to stronger interactions.[11] Although the larger size of the TiO_2 particles may also play a role, they suggest that the bound layer thickness would also be affected by other factors, such as the properties of filler and polymer. How those factors act together to influence the bound layer thickness is what really matters in the study of this bound layer mechanism and is investigated herein.

In this letter, dielectric relaxation spectroscopy (DRS) in the frequency range of 10^{-1} to 10^{7} Hz is used to investigate the segmental relaxation of poly-2-vinylpyridine (P2VP) with silica nanoparticles, whose interaction with P2VP is strong.[7,12] The thickness of the bound polymer layer surrounding each silica nanoparticle is estimated from the reduction in the magnitude of the segmental relaxation in the presence of silica nanoparticles with different sizes and loadings. The bound layer thickness is found to weakly increase with particle size and this finding is discussed in relation to changes in interfacial curvature.

Nanocomposite systems containing silica nanoparticles (generously donated by Nissan Chemicals), with radii of R = 7, 11.5, 25, and 50 nm, well-dispersed in the P2VP matrix (M_w = 105000; M_w/M_n = 1.08; T_g = 98 °C; Polymer Source, Inc.)

Received: April 27, 2014
Accepted: July 11, 2014
Published: July 24, 2014

   dx.doi.org/10.1021/mz500252f | ACS Macro Lett. 2014, 3, 773−777

are investigated at various concentrations. The samples were prepared by solution casting from either 2-butanone (for R = 7 and 25 nm particles) or isopropanol (for R = 11.5 and 50 nm particles) with pyridine (Sigma-Aldrich) as dispersant (pyridine acts as a Lewis base, accepting a proton from silica, leaving silica with a negative charge and pyridinium counterions, that charge-stabilize nanoparticles in solution.). Ultrasonication was applied during the mixing of silica and P2VP in solution to improve dispersion. After removal of the solvent, the polymer nanocomposites were then characterized by transmission electron microscopy (TEM) to determine the dispersion state of the nanoparticles in the polymer matrix. The samples were then molded into thin discs at 150 °C and sandwiched between two freshly polished brass electrodes with diameters of 15 and 25 mm for the dielectric measurements. Samples were annealed under vacuum at 120 °C for 12 h prior to the measurements on a Novocontrol GmbH Concept 40 Broadband Dielectric Spectrometer with a Quatro temperature control system (temperature precision of 0.1 °C). The dielectric data were normalized by requiring the same dielectric permittivity at the highest frequency. This normalization is needed to correct for minor changes of sample thickness/electric capacity due to the thermal expansion during the measurements.

Figure 1a shows the angular frequency dependence of dielectric loss ε'' from 120 to 170 °C for nanoparticles of radius

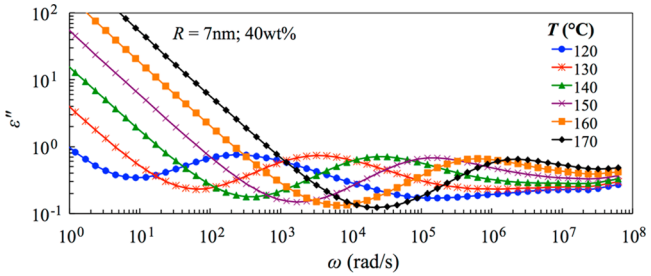

Figure 1. Dielectric loss ε'' (ω) as a fucntion of angular frequency ω from 120 to 170 °C for a nanocomposite melt comprised of 40 wt % of R = 7 nm silica in P2VP.

R = 7 nm and weight fraction w = 40 wt % in P2VP/silica nanocomposites. The main peak is assigned to the segmental α relaxation. Toward the low frequency side, the DC conductivity is evident as $\varepsilon'' \sim 1/\omega$. The broadening at the highest frequencies is due to more separated α and β processes at lower T, because the incoming β-relaxation has weaker temperature dependence than the α-relaxation (A comparison of the dielectric mode distribution at different T is shown in Figure S1 of Supporting Information). Therefore, different nanocomposites are examined at a single T = 130 °C = T_g + 32 °C, where the α-relaxation can be fully resolved and cleanly separated from the conductivity at lower frequency and the β-relaxation at higher frequency.

The frequency-domain Havriliak–Negami (HN) function is used to fit the dielectric segmental relaxation of polymers and other glass-forming liquids.[13]

$$\varepsilon^*(\omega) = \varepsilon_\infty + \frac{\Delta\varepsilon}{[1 + (i\omega\tau_{HN})^\alpha]^\gamma} \quad (1)$$

ε_∞ is the dielectric permittivity at high frequency before the α-relaxation, $\Delta\varepsilon$ is the dielectric relaxation strength of the α-relaxation, while α and γ are the two shape parameters of the HN function.

The HN function (eq 1 with four parameters) can approximate the frequency domain counterpart of the Kolrausch–Williams–Watts (KWW) function in the time domain (with only three parameters) using an additional restriction on the two shape parameters α and γ (eq 2), as derived by Alvarez et al.[14]

$$\gamma = 1 - 0.812(1 - \alpha)^{0.387} \quad (2)$$

$$\beta = (\alpha\gamma)^{1/1.23} \quad (3)$$

With this constraint in place, the fits involve three parameters: the HN characteristic time τ_{HN}, the β stretching exponent and the dielectric strength $\Delta\varepsilon$. Since the dielectric loss of the α-relaxation is affected by conductivity at low ω, their fitting to the KWW equation is done on the derivative formalism defined as $\varepsilon_{der}(\omega) = -\pi/2 \times d\varepsilon'(\omega)/d \ln \omega$.[15]

Figure 2 shows ε_{der} of the α-relaxations at T = 130 °C for P2VP/silica nanocomposites with the same nanoparticle radius R = 7 nm at different NP weight fractions w (from 0 to 60 wt %), as indicated. The symbols are the experimental results multiplied by a factor of A as indicated, to avoid overlapping of the plots. For w = 0, the red curve is the KWW fit of pure P2VP

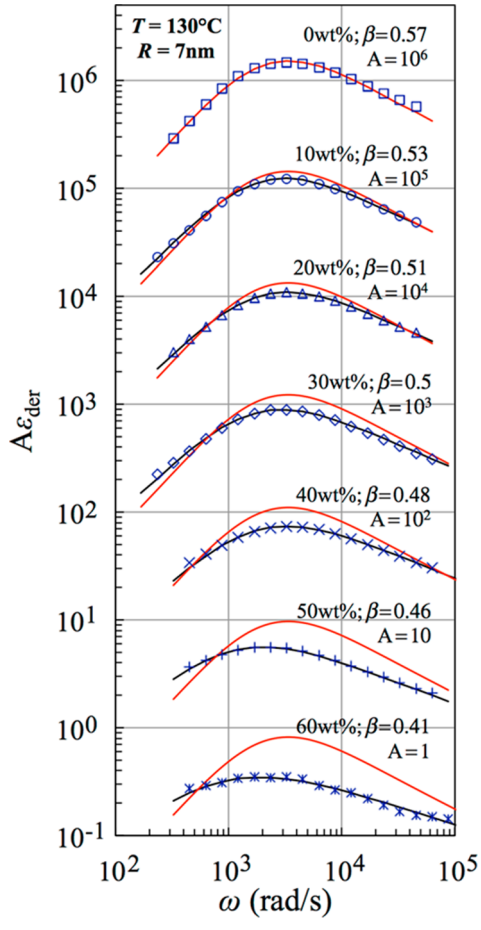

Figure 2. Dielectric derivative spectra $\varepsilon_{der}(\omega) = -\pi/2 \times d\varepsilon'(\omega)/d \ln \omega$ at T = 130 °C (symbols) for nanocomposites with the same particle radius R = 7 nm and different weight fractions w as indicated, multiplied by scale factor A for clarity, also indicated. Pure P2VP (top curve) is fit to KWW (red curve) to obtain $\varepsilon_{der,P2VP}$ and $\phi_{P2VP}\varepsilon_{der,P2VP}$ is compared with each data set as the red curves. Finally, KWW fits of P2VP/silica nanocomposites (black curves with β as indicated) are added for comparison.

dx.doi.org/10.1021/mz500252f | ACS Macro Lett. 2014, 3, 773–777

with β = 0.57. For comparison, that KWW fit of pure P2VP $\varepsilon_{der,P2VP}$ is multiplied by the volume fraction of P2VP in the system, $\phi_{P2VP} = (1 - w)/\rho_{P2VP}/[w/\rho_{particle} + (1 - w)/\rho_{P2VP}]$ with the density ρ_{P2VP} = 1.15 g/cm^3 and $\rho_{particle}$ = 2.2 g/cm^3, and added for comparison with experimental results at each w, as the red curves. Compared with $\phi_{P2VP}\varepsilon_{der,P2VP}$, the experimental ε_{der} shows broader distribution and lower intensity as loading fraction is increased.

To quantify the change after adding particles, the experimental results are fit with β, $\Delta\varepsilon$, and τ_{HN} as three fitting parameters. The dielectric strength of the segmental relaxation, $\Delta\varepsilon$, directly measures the amount of free polymer, assuming there is no difference between the dielectric strength per unit volume of the bulk polymer and nanocomposite matrix. Therefore, by comparing the difference between $\Delta\varepsilon$ of P2VP and P2VP/silica, the volume fraction of free polymer in nanocomposites can be calculated:

$$\phi_{free} = \frac{\Delta\varepsilon}{\Delta\varepsilon_{P2VP}} \tag{4}$$

Since the system consists of only nanoparticles, polymer in the bound layer and free polymer, $(1 - \phi_{free})/\phi_{particle}$ corresponds to a ratio of volumes of a particle + bound layer shell and that of the particle alone. Then, the radius of each nanoparticle + bound layer shell is $[(1 - \phi_{free})/\phi_{particle}]^{1/3}R$, and the bound layer thickness is

$$\delta = R\left\{\left(\frac{1 - \phi_{free}}{\phi_{particle}}\right)^{1/3} - 1\right\} \tag{5}$$

In eq 5, each particle is assumed to be identical and homogeneously dispersed, as confirmed in TEM measurements (see Figure 3b–d) where no particle clusters are observed for filler with R = 11.5, 25, and 50 nm, even at the high loading fraction of w = 40 wt %.

Figure 3a shows the calculated bound layer thickness δ for all the P2VP/silica nanocomposites, having R = 7, 11.5, 25, and 50 nm at T = 130 °C, plotted against weight percent of silica. The

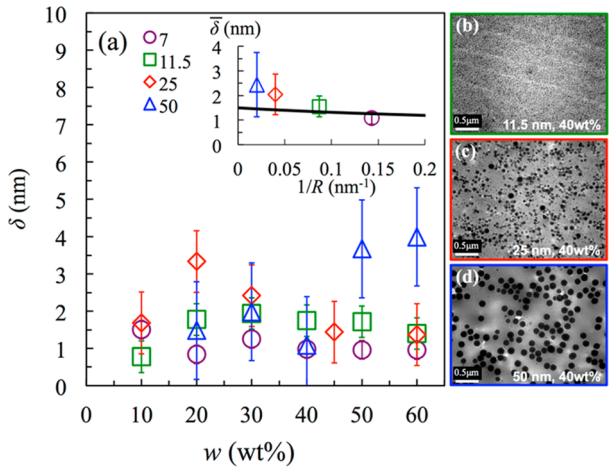

Figure 3. (a) Bound layer thickness δ (calculated at reference temperature 130 °C) as a function of particle weight percent w. Inset: Average bound layer thickness $\bar{\delta}$ as a function of particle radius R. Solid line is prediction of eq 6 with δ_∞ = 1.5 nm. Right panels: (b–d) TEM images of P2VP/silica nanocomposites with different radius R = 11.5, 25, and 50 nm at the same high loading w = 40 wt %.

uncertainty of δ decreases with decreasing particle size, leading to more particle–polymer interface per unit volume. It is noted that the bound layer thickness is not sensitive to a change of loading fraction, possibly because the particles are well separated even at high loading (see TEM images in Figure 3). In the inset of Figure 3a, the average of δ for the same particle at different loading fraction, $\bar{\delta}$, is plotted against reciprocal particle radius $1/R$: It is noted that $\bar{\delta}$ is in a range of 1 to 2.5 nm and decreases slightly with decreasing R.

One possible explanation for this decrease is the curvature of the particles. To explain the role of curvature, consider a simple case where a unit of interface is assumed to confine a fixed amount of segments. Assume a bound layer of thickness δ_∞ can be formed for a flat interface. Then, for a particle of radius R, the volume of confined segments is $\delta_\infty 4\pi R^2$, leading to a volume of a particle + bound layer shell $4\pi R^3/3 + \delta_\infty 4\pi R^2$, and bound layer thickness:

$$\delta(R) = (3R^2\delta_\infty + R^3)^{1/3} - R \tag{6}$$

Note that $\delta(R) = \delta_\infty$ when $R \gg \delta_\infty$, where a flat interface can be assumed. In the inset of Figure 3a, the curve is $\delta(R)$ calculated from eq 6 with δ_∞ = 1.5 nm, the Kuhn segment length of P2VP. This simple calculation reflects the trend observed for the particle size dependence of average bound layer thickness. Nevertheless, one should note that the decrease of $\bar{\delta}$ with R is stronger than the simple prediction, meaning a unit area of the more curved surface effectively confines a smaller amount of segments than a unit area of the flatter surface.

To further check this point, in Figure 4a, the KWW shape parameter β is plotted against loading fraction w. Note that β decreases with increasing loading and also with decreasing R, both leading to larger total surface area of particles per unit volume. Figure 4b tries to normalize the change of interface area per unit volume for different particle sizes: since the average surface area of particles per unit volume of nanocomposites can be written as $A_V = \phi_{particle}S/V$, where $S = 4\pi R^2$ and $V = 4\pi R^3/3$ are the surface area and volume per particle, respectively, leading to $A_V = 3\phi_{particle}/R$. In Figure 4b, β is plotted against $A_V = 3\phi_{particle}/R$. At the same A_V, β is lower for larger R, meaning that larger particles broaden the segmental mode distribution more after A_V has been properly normalized. This result is in accordance with a conclusion from the inset of Figure 3: a unit area of flatter surface can constrain more polymer segments.

Figure 5 compares the bound layer thicknesses obtained for PDMS/silica,[11] PDMS/titania,[11] and P2VP/silica from DRS, and for P2VP/silica from thermogravimetric analysis (TGA).[12] (In ref 12, dynamic light scattering (DLS) and transmission electronic microscopy (TEM) were used to determine the size of the absorbed polymer layer that increases with the radius of gyration of the polymer chains. The adsorbed layer is not compared in Figure 5 because it is conceptually different from the bound layer determined in this study.) Interestingly, the bound layer thickness extracted from TGA is comparable to that from DRS, meaning that the chains with segments strongly adsorbed to the particles are comparable to those being immobilized. The bound layer thickness is comparable to the Kuhn length (=1.5 nm) of adsorbed polymer and decreases as smaller particles are used. For PDMS/silica and PDMS/titania, the overall trend is the same: δ increases weakly with R. Klonos et al. argued that the particle/polymer energetic interactions are stronger in the case of titania/PDMS than silica/PDMS, leading

dx.doi.org/10.1021/mz500252f | ACS Macro Lett. 2014, 3, 773–777

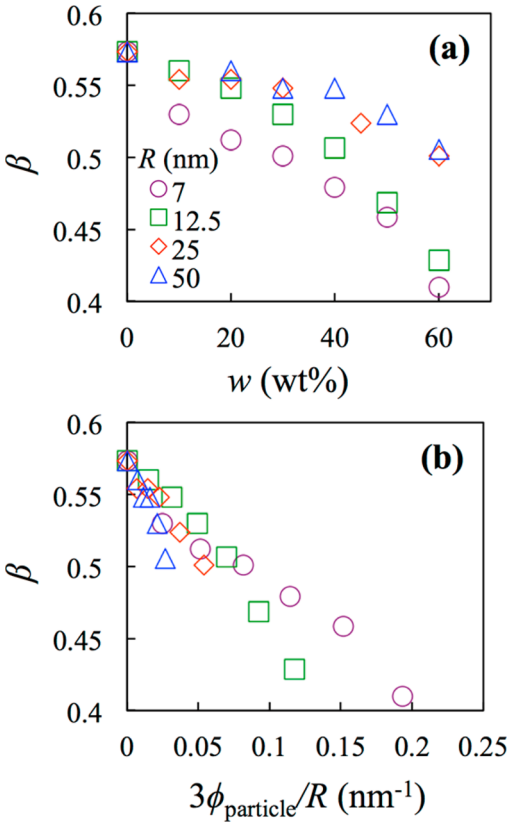

Figure 4. (a) KWW shape parameter β as a function of particle weight fraction w for the P2VP/silica nanocomposites with R, as indicated at T = 130 °C. (b) KWW shape parameter β at 130 °C as a function of the total particle surface area per unit volume $3\phi_{particle}/R$.

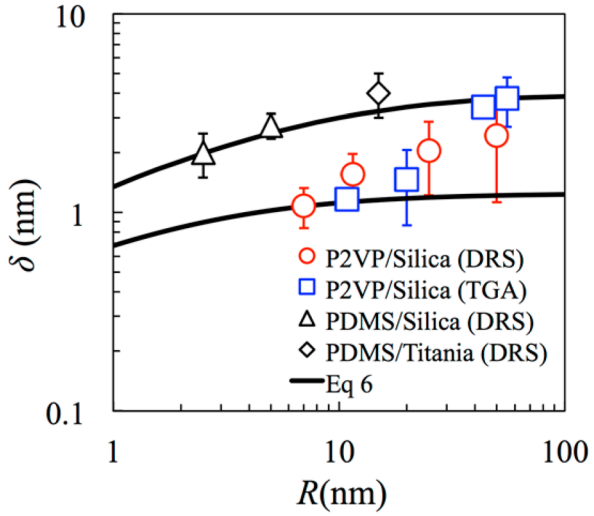

Figure 5. (a) Bound layer thickness δ as a function of particle radius R for the P2VP/silica inferred from DRS and TGA;[12] PDMS/silica[11] and PDMS/titania[11] inferred from DRS; predictions from eq 6 (solid curves) with bound layer thickness on a flat surface δ_∞ = 1.25 (estimated lower bound) and 4 nm (estimated upper bound).

to the larger δ for the former.[11] Nevertheless, they utilized larger titania particles than silica particles, and this size difference may account for their observations.

Predictions of eq 6 (thick solid curves in Figure 5, also shown in the inset of Figure 3) capture the overall trend: all experimental data are bracketed in two sets of predictions at two limiting conditions δ_∞ = 1.25 (lower bound) and 4 nm (upper bound). In comparison to the predictions, δ decreases more abruptly with R in DRS and TGA, meaning a unit of more curved interface immobilizes fewer segments. The stronger decrease of δ with R revealed in the experiments suggests two important points for application of nanocomposites: (1) a possibility to tune the bound layer thickness by changing the size of nanoparticles and (2) sufficiently small particles (smaller than R = 7 nm) might have negligible bound layer and act simply as plasticizers for the polymer matrix.

Recently, Holt et al. also evaluated the bound layer thickness via DRS for similar P2VP/silica nanocomposites.[16] They concluded an interfacial thickness of δ = 4−6 nm for nanoparticles with R = 15 nm, which is more than two times the bound layer thickness determined in the current study. Holt et al. separate the broadened dielectric α process into two overlapping parts; a component far from the particles that is unaffected (but smaller in magnitude) by the particles and a very broad bound layer process (see Figure 4d in ref 16). Their assumption thus naturally leads to a significantly thicker bound layer estimation. Herein the analysis is based on a single process broadening as particles are added and attributes the reduction of dielectric intensity to immobile segments in the bound layer. There is also a far slower dielectric process in ε_{der}, detailed in Figure S2 in Supporting Information, as reported by Papadopoulos et al.[17] for pure P2VP and noted also in Holt et al.'s work (Figure 4b in ref 16), whose origins are unclear but has been suggested to originate from charge separation[18] and there is no trend of the magnitude of this slower process with particle loading.

In summary, dielectric relaxation spectroscopy was used to study the main segmental α relaxation of a series of silica hydrophilic nanoparticles in polar P2VP polymer matrices with various silica sizes and concentrations. It is noted that smaller silica particles and higher filler concentrations slow down and broaden the segmental relaxation significantly. Furthermore, dielectric intensity of the α-relaxation is lower for nanocomposites than that expected from the volume fraction of the polymer matrix and dielectric strength of the bulk P2VP. The decrease of dielectric intensity is attributed to segments immobilized in the bound layer, thereby allowing an evaluation of the bound layer thickness by dielectric relaxation spectroscopy. The relationship between the bound layer thickness and particle size suggests a possibility to tune the bound layer thickness by changing the size of the nanoparticles.

■ ASSOCIATED CONTENT

Supporting Information

Figure S1: Comparison of DRS spectra at different T; Figure S2: T dependencies for ε'' of P2VP and the nanocomposites; Figure S3: Dielectric derivative formalism of P2VP bulk and nanocomposites in the frequency range 10^{-1} rad/s to 10^{5}rad/s. This material is available free of charge via the Internet at http://pubs.acs.org.

■ AUTHOR INFORMATION

Author Contributions

†Cofirst authors (S.G. and Q.C.).

Notes

The authors declare no competing financial interest.

dx.doi.org/10.1021/mz500252f | ACS Macro Lett. 2014, 3, 773−777

■ ACKNOWLEDGMENTS

The authors gratefully acknowledge the financial support of the National Science Foundation Grant DMR-1006659.

■ REFERENCES

(1) Lin, F.; Bhatia, G. S.; Ford, J. D. *J. Appl. Polym. Sci.* **1993**, *49*, 1901−1908. Usuki, A.; Kojima, Y.; Kawasumi, M.; Okada, A.; Fukushima, Y.; Kurauchi, T.; Kamigaito, O. *J. Mater. Res.* **1993**, *8*, 1179−1184. Giannelis, E. P. *Adv. Mater.* **1996**, *8*, 29−35. Alexandre, M.; Dubois, P. *Mater. Sci. Eng., R* **2000**, *28*, 1−63. Sanchez, C.; Soler-Illia, G.; Ribot, F.; Lalot, T.; Mayer, C. R.; Cabuil, V. *Chem. Mater.* **2001**, *13*, 3061−3083. Ray, S. S.; Okamoto, M. *Prog. Polym. Sci.* **2003**, *28*, 1539−1641.

(2) Chouchaoui, C. S.; Benzeggagh, M. L. *Compos. Sci. Technol.* **1997**, *57*, 617−622.

(3) Rittigstein, P.; Priestley, R. D.; Broadbelt, L. J.; Torkelson, J. M. *Nat. Mater.* **2007**, *6*, 278−282. Liu, X.; Wu, Q. *Polymer* **2001**, *42*, 10013−10019. Fragiadakis, D.; Pissis, P.; Brozova, L. *Polymer* **2005**, *46*, 6001−6008. Ash, B.; Schadler, L.; Siegel, R. *Mater. Lett.* **2002**, *55*, 83−87. Bershtein, V.; Egorova, L.; Yakushev, P.; Pissis, P.; Sysel, P.; Brozova, L. *J. Polym. Sci., Part B: Polym. Phys.* **2002**, *40*, 1056−1069. Chen, K.; Yang, S. *J. Appl. Polym. Sci.* **2002**, *86*, 414−421.

(4) Bogoslovov, R. B.; Roland, C. M.; Ellis, A. R.; Randall, A. M.; Robertson, C. G. *Macromolecules* **2008**, *41*, 1289−1296.

(5) Trombly, D. M.; Ganesan, V. *J. Chem. Phys.* **2010**, *133*, 154904−154910. Kalb, J.; Dukes, D.; Kumar, S. K.; Hoy, R. S.; Grest, G. S. *Soft Matter* **2011**, *7*, 1418−1425.

(6) Pandey, Y. N.; Doxastakis, M. *J. Chem. Phys.* **2012**, *136*, 094901−094910.

(7) Harton, S. E.; Kumar, S. K.; Yang, H.; Koga, T.; Hicks, K.; Lee, H. K.; Mijovic, J.; Liu, M.; Vallery, R. S.; Gidley, D. W. *Macromolecules* **2010**, *43*, 3415−3421.

(8) Meissner, B. *J. Appl. Polym. Sci.* **1974**, *18*, 2483−2491.

(9) Garvey, M. J.; Tadros, T. F.; Vincent, B. *J. Colloid Interface Sci.* **1976**, *55*, 440−453.

(10) Baker, J. A.; Pearson, R. A.; Berg, J. C. *Langmuir* **1989**, *5*, 339−342.

(11) Klonos, P.; Panagopoulou, A.; Bokobza, L.; Kyritsis, A.; Peoglos, V.; Pissis, P. *Polymer* **2010**, *51*, 5490−5499. Fragiadakis, D.; Pissis, P.; Bokobza, L. *J. Non-Cryst. Solids* **2006**, *352*, 4969−4972.

(12) Jouault, N.; Moll, J. F.; Meng, D.; Windsor, K.; Ramcharan, S.; Kearney, C.; Kumar, S. K. *ACS Macro Lett.* **2013**, *2*, 371−374.

(13) Havriliak, S.; Negami, S. *Polymer* **1967**, *8*, 161−205.

(14) Alvarez, F.; Alegria, A.; Colmenero, J. *Phys. Rev. B* **1991**, *44*, 7306−7312. Alvarez, F.; Alegria, A.; Colmenero, J. *Phys. Rev. B* **1993**, *47*, 125−130.

(15) Boersma, A.; van Turnhout, J.; Wubbenhorst, M. *Macromolecules* **1998**, *31*, 7453−7460.

(16) Holt, A. P.; Griffin, P. J.; Bocharova, V.; Agapov, A. L.; Imel, A. E.; Dadmun, M. D.; Sangoro, J. R.; Sokolov, A. P. *Macromolecules* **2014**, *47*, 1837−1843.

(17) Papadopoulos, P.; Peristeraki, D.; Floudas, G.; Koutalas, G.; Hadjichristidis, N. *Macromolecules* **2004**, *37*, 8116−8122.

(18) Richert, R.; Agapov, A.; Sokolov, A. P. *J. Chem. Phys.* **2011**, *134*, 104508.